Hydrol. Earth Syst. Sci. Discuss., 11, 1169–1201, 2014
www.hydrol-earth-syst-sci-discuss.net/11/1169/2014/
doi:10.5194/hessd-11-1169-2014

Hydrology and Earth System Sciences
Open Access
Discussions

Evaluation of TRMM rainfall estimates over a large Indian river basin (Mahanadi)

D. Kneis[1], **C. Chatterjee**[2], **and R. Singh**[2]

[1]University of Potsdam, Inst. of Earth and Environmental Sciences, Potsdam, Germany
[2]Indian Institute of Technology at Kharagpur, Agricultural and Food Eng. Dept., Kharagpur, India

Received: 22 November 2013 – Accepted: 10 January 2014 – Published: 23 January 2014

Correspondence to: D. Kneis (david.kneis@uni-potsdam.de)

Published by Copernicus Publications on behalf of the European Geosciences Union.

Abstract

The paper examines the quality of satellite-based precipitation estimates for the Lower Mahanadi River Basin (Eastern India). The considered data sets known as 3B42 and 3B42-RT (version 7/7A) are routinely produced by the tropical rainfall measuring mission (TRMM) from passive microwave and infrared recordings. While the 3B42-RT data are disseminated in real time, the gage-adjusted 3B42 data set is published with a delay of some months. The quality of the two products was assessed in a two-step procedure. First, the correspondence between the remotely sensed precipitation rates and rain gage data was evaluated at the sub-basin scale. Second, the quality of the rainfall estimates was assessed by analyzing their performance in the context of rainfall-runoff simulation.

At sub-basin level (4000 to 16 000 km^2) the satellite-based areal precipitation estimates were found to be moderately correlated with the gage-based counterparts (R^2 of 0.64–0.74 for 3B42 and 0.59–0.72 for 3B42-RT). Significant discrepancies between TRMM data and ground observations were identified at high intensity levels. The rainfall depth derived from rain gage data is often not reflected by the TRMM estimates (hit rate < 0.6 for ground-based intensities > 80 mm day^{-1}). At the same time, the remotely sensed rainfall rates frequently exceed the gage-based equivalents (false alarm ratios of 0.2–0.6). In addition, the real time product 3B42-RT was found to suffer from a spatially consistent negative bias.

Since the regionalization of rain gage data is potentially associated with a number of errors, the above results are subject to uncertainty. Hence, a validation against independent information, such as stream flow, was essential. In this case study, the outcome of rainfall–runoff simulation experiments was consistent with the above-mentioned findings. The best fit between observed and simulated stream flow was obtained if rain gage data were used as model input (Nash–Sutcliffe Index of 0.76–0.88 at gages not affected by reservoir operation). This compares to the values of 0.71–0.78 for the gage-adjusted TRMM 3B42 data and 0.65–0.77 for the 3B42-RT real-time data.

HESSD
11, 1169–1201, 2014

Whether the 3B42-RT data are useful in the context of operational runoff prediction in spite of the identified problems remains a question for further research.

1 Introduction

Precipitation estimates constitute the essential forcing of hydrological catchment models. Reliable data on rain and snowfall are indispensable for model calibration, simulation, and forecasting. In many regions of the world, rain gage data are difficult to access for technical and/or administrative reasons. This is particularly true for real-time data needed for operational hydrological forecasting. In many catchments, precipitation estimates are also subject to considerable uncertainty due to the small number of rain gages and/or non-representative observation sites. Finally, recording devices, human operators, and data transmission are susceptible to errors and outages for various reasons. Therefore, traditional precipitation records are rarely complete.

In view of these difficulties, the use of remotely-sensed precipitation estimates becomes attractive. In large river basins, satellite-based estimates are of particular interest. For latitudes $\leq 50^{\circ}$, such data are made available at no charge by the TRMM mission, jointly conducted by the US and Japanese space agencies. The TRMM product with identifier 3B42 is particularly suitable for hydrological modeling due to its high resolution in space ($0.25^{\circ} \times 0.25^{\circ}$) and time (3 h). In addition to ground-adjusted data for research purposes (Huffman et al., 2007), a near real-time variant known as 3B42-RT is available (Huffman and Bolvin, 2013).

TRMM-based precipitation estimates were compared to rain gage measurements in a number of case studies from all over the world (see, e.g. Oke et al., 2009; Javanmard et al., 2010; Liu et al., 2012; Ouma et al., 2012; Gao and Liu, 2013; Peña-Arancibia et al., 2013). A preliminary evaluation over India was carried out by Rahman and Sengupta (2007) at daily scale using a spatial resolution of $1^{\circ} \times 1^{\circ}$. TRMM data were also tried as inputs for hydrological modeling by a number of groups (Collischonn et al.,

HESSD
11, 1169–1201, 2014

2008; Li et al., 2012). Regarding India, the suitability of TRMM-based precipitation data for hydrological modeling is yet to be studied for most river basins.

This paper analyzes the latest TRMM 3B42 (version 7) and 3B42-RT (version 7, revision 2) data for a hydrologically sensitive part of India. The spatial focus is on the Mahanadi River Basin downstream of the Hirakud Reservoir. To our knowledge, no case study on the quality of TRMM data is available for this specific area. The evaluation is carried out in two steps. First, the satellite-based precipitation estimates are compared to ground observations after spatial and temporal aggregation. Second, TRMM and rain gage data are processed through a hydrological model and the corresponding errors in simulated stream flow are analyzed.

2 Study area

The Mahanadi River Basin covers an area of about 140 000 km^2 in the Eastern part of India. The Mahanadi and its tributaries drain a considerable part of the states Chhattisgarh and Orissa towards the Bay of Bengal. In the delta region, the river is split across a number of branches, including man-made canals. According to the global land-cover data set (JRC, 2003), 55 % of the basin is covered by agricultural land of which almost 90 % is subject to irrigation. Forests and shrubs cover 35 and 7 %, respectively. Built-up areas are of minor importance.

The basin's climate is characterized by the Monsoon with dry winters and wet summers. Rainfall amounts to approx. 1500 mm yr^{-1}. The annual peak is typically observed in July with about 400 mm $month^{-1}$. In the dry season extending from November to March, rainfall is usually less than 20 mm $month^{-1}$. The annual maximum of air temperature occurs in May with average values well above 30 °C.

The flow regime in the lower reaches of the Mahanadi River is largely controlled by the Hirakud Dam operated since 1957 (Fig. 1). The Hirakud reservoir serves multiple purposes such as flood protection of the delta region, irrigation, and power production. With a storage capacity of over 5 km^3, Hirakud is one of India's largest reservoirs. In

HESSD
11, 1169–1201, 2014

spite of its significant retention capacity, the lower reaches of the Mahanadi River still experience severe floods associated with significant losses (DOWR, 2009). The latest major events occurred in 1980, 1982, 2008, and 2011 with peak discharges of up to 44 000 $m^3 s^{-1}$ entering the delta downstream of Mundali (easternmost gage in Fig. 1). Peak travel times from Hirakud to Mundali (310 km) range from 36 to 50 h (DOWR, 2010).

3 Data and methods

3.1 Precipitation data sets

3.1.1 TRMM rainfall estimates

Two high-resolution rainfall data sets provided by the TRMM mission were analyzed. The official identifiers are 3B42 for the gage-adjusted research version and 3B42-RT for the real-time variant. Basic facts about the two data sets are collected in Table 1. A description of the remote sensing approach and technical specifications can be found in Huffman et al. (2007) for the 3B42 data and Huffman and Bolvin (2013) for the 3B42-RT data. The two data sets can be downloaded from the NASA servers disc2.nascom.nasa.gov/s4pa/TRMM_L3/TRMM_3B42 and trmmopen.gsfc.nasa.gov/pub/merged/3B42RT, respectively.

The spatial coverage of the Mahanadi Basin by the TRMM grid is illustrated in Fig. 2. In this region, the dimensions of an individual 0.25° × 0.25° grid cell is about 26 km × 28 km (≈ 730 km^2). The number of missing values in the TRMM times series is surprisingly low. In over 12 yr, the real-time data set is incomplete on 28 days only. On all but two days the spatial coverage is at least 50 %.

The data were downloaded using the software tool “wget” after collecting a list of all required file paths. Appropriate R scripts were used for the purpose of further processing, including decompression, conversion to ASCII, spatial subsetting, time

HESSD
11, 1169–1201, 2014

conversions, and formatting. The actual binary-to-ASCII conversion was performed using "hdp" (for HDF files) and customized C code (for the 3B42-RT file format). The correctness of the processing was verified by plotting the results for selected dates. Spatial patterns and the scaling were then compared to corresponding outputs of the NASA's online visualization system "TOVAS".

The 3B42-RT product showed a moderate negative bias when compared with the gage-adjusted 3B42 product. A bias-corrected version was obtained by multiplying the original 3B42-RT data with an appropriate adjustment factor. To retain the character of a real-time product which does not depend on recent retrospective information, correction factors were derived for two independent sub-sets of the 11 yr time series. The factor determined on the first half of the time series was applied to the second half and vice versa.

3.1.2 Rain gage data

Daily rainfall data were provided by the India Meteorological Department for 74 rain gages located inside and nearby the Lower Mahanadi Basin (Fig. 2). Implausible values and periods with zero-only data during the monsoon season were marked as "missing". Furthermore, the data at all rain gages were validated by double mass analysis using the spatial median as the reference. Based on this, the data of some rain gages and/or years were also set to "missing". To facilitate further analysis and the use of the data as a model input, all "missing" values were finally substituted with estimates obtained by spatial interpolation (inverse distance method).

3.1.3 Disaggregated gage data

A derived, gage-based precipitation estimate was obtained by imprinting the 3 hourly pattern of the TRMM 3B42 data on the 24 h sums observed at the rain gages. The approach of disaggregation is described by Eq. (1). In this equation, G3 is the 3 hourly estimate for a gage, G24 is the original daily observation, and SRR_3 and SRR_{24} denote

HESSD
11, 1169–1201, 2014

the corresponding 3 hourly and daily sums according to the real-time TRMM data for the nearest grid cell (cf. Table 2).

$$G3 = \begin{cases} G24 \cdot SRR_3/SRR_{24} & \text{if } SRR_{24} > 0 \\ G24 \cdot 3/24 & \text{if } SRR_{24} = 0 \end{cases} \quad (1)$$

3.1.4 Short data set identifiers

For clarity, abbreviations are introduced to identify the various precipitation estimates introduced in the previous sections. Gage-based estimates are generally identified by the initial letter "G" whereas an initial "S" is used for the satellite-based estimates. A summary of all abbreviations used throughout the remainder of the paper is given in Table 2.

3.2 Evaluation procedure

First, the correspondence between the satellite-based precipitation estimates and rain gage data was examined. For that purpose, the data were aggregated in space (areal rainfall for sub-basins) and time (24 h sums). The spatial aggregation aims at compensating for the coarse resolution of the TRMM grid (Fig. 2) compared with the rain gage domain. The temporal aggregation was necessary since high resolution rain gage data were unavailable. The association of the data sets was expressed in terms of R^2 and the percentage bias (Eq. 5). The probability of detection (POD), the false alarm ratio (FAR) and the equitable threat score (ETS) were evaluated to assess the ability of the remote sensing approach to properly detect high rainfall intensities. For a contingency table like Table 3, these first two scores are defined by Eqs. (2) and (3). See Jolliffe and Stephenson (2003) for the definition of ETS.

HESSD
11, 1169–1201, 2014

$$\mathrm{POD} = \frac{\mathrm{Hits}}{\mathrm{Hits} + \mathrm{Misses}} \tag{2}$$

$$\mathrm{FAR} = \frac{\mathrm{False\ Alarms}}{\mathrm{Hits} + \mathrm{False\ Alarms}} \tag{3}$$

Second, rain gage data and satellite-based estimates were processed through a conceptual hydrological model. This allowed for a comparison of the rainfall estimates with respect to the error of simulated runoff. The error was quantified by the Nash–Sutcliffe Index, NS, and the percentage bias, pBias (Eqs. 4 and 5; $\boldsymbol{o}$: observations, $\boldsymbol{p}$: model predictions, MSE: mean squared error, VAR: variance operator, n: length of vectors $\boldsymbol{o}$ and $\boldsymbol{p}$). Since systematic errors in rainfall input may partly be compensated by the choice of the model's parameters (see, e.g. Heistermann and Kneis, 2011), the evaluation was done with and without (re-)calibration of the hydrological model to the individual rainfall data sets.

$$\mathrm{NS} = 1 - \frac{\mathrm{MSE}(\boldsymbol{p}, \boldsymbol{o})}{\mathrm{VAR}(\boldsymbol{o})} \tag{4}$$

$$\mathrm{pBias} = \frac{\sum_{i=1}^{n} (p_i - o_i)}{\sum_{i=1}^{n} (o_i)} \cdot 100\,\% \tag{5}$$

The evaluation was carried out on the period March 2000 to December 2010 owing to the limited access to hydrological and rain gage data. For the same reason, the spatial focus was put on the Lower Mahanadi Basin downstream of the Hirakud dam.

HESSD
11, 1169–1201, 2014

3.3 Hydrological modeling

3.3.1 Model engine

The hydrological model used in this study is called HYPSO-RR. This is a time-continuous, semi-distributed, conceptual model developed on the basis of the ECHSE modeling framework. Both the model and the underlying modeling framework are available at http://echse.bitbucket.org including source code and documentation.

The basic *types of* objects (formally called *classes*) simulated by HYPSO-RR are (1) sub-basins, (2) river reaches, and (3) river junctions. Additional classes are available for the simulation of lakes and reservoirs. HYPSO-RR was originally designed for time-consuming applications in hydrological forecasting (ensemble simulation, operational data assimilation). Therefore, computational efficiency was given priority over a very detailed, strictly physically-based description of real-world processes. A brief summary of the major hydrological processes and the associated model concepts is presented in Table 4. A detailed documentation, including all equations, can be found in Kneis (2012b). The current version of HYPSO-RR distinguishes three classes of land cover only: vegetated soil, water, and impervious surfaces.

3.3.2 Spatial setup and data

Drainage network and watershed boundaries were derived from the ASTER digital elevation model using software described in Kneis (2012b). The median sub-basin size was about 150 km^2. Information on land use was taken from the global land cover map (JRC, 2003). Basic soil properties were extracted from the global WISE data base provided by the International Soil Reference and Information Centre (www.isric.org).

Survey cross-section data were available for 40 sites along the main Mahanadi River between Hirakud and Mundali. For about 200 additional sites, cross-sections were extracted from the elevation model. Based on this information, hydraulic parameters

HESSD
11, 1169–1201, 2014

were assigned to all simulated reaches using the regionalization approach described in Kneis (2012b).

3.3.3 Meteorological inputs

The rainfall data sets introduced in Sects. 3.1.2 and 3.1.1 form the essential input of the hydrological model. Both the gage and satellite data were interpolated to the sub-basins' centers of mass using inverse-distance weighting (power: 2, max. number of neighbors: 4, search sectors: 4).

In addition to rainfall data, HYPSO-RR requires time series of air temperature, short-wave radiation, and air-pressure, at least. The available temperature data (5 stations, daily records) were regionalized by residual interpolation using the sub-basins' elevation as external predictor. Radiation data were accessible for a single station only (monthly averages). Air-pressure was generally estimated from elevation.

3.3.4 Observed stream flow

Stream flow data were provided by India's Central Water Commission for the gages listed in Table 5. Most of the hydrographs consist of instantaneous values recorded at 08:00 IST. Hourly data existed for Mundali only. Information on the release from the Hirakud Reservoir was available as 24 h averages. Knowledge of the discharge at Hirakud is essential for simulating stream flow in the downstream reaches of the Mahanadi River, including the gaging sites Tikarpara and Mundali.

3.3.5 Calibration strategy

The calibration of the hydrological model was performed semi-automatically using a sequence of Monte Carlo simulations (SMCS). This approach was tested in a number of rainfall-runoff modeling studies (e.g. Kneis et al., 2012). It is briefly described by the following algorithm:

HESSD
11, 1169–1201, 2014

1. Define initial sampling ranges for all parameters based on physical limits, literature, data analysis, or experience from earlier studies.
2. Generate *n* random parameter sets by the Latin Hypercube method with uniform distribution.
3. Run the model for all parameter sets and compute the objective function, i.e. the simulation error.
4. Plot the objective function's value against the individual parameter values.
5. Visually inspect the plots and narrow (or shift) the sampling ranges where an optimum (or trend) can be identified with sufficient certainty.
6. Continue with step 2 until all sampling ranges have collapsed to zero width.

With respect to the HYPSO-RR model engine, initial estimates for many parameters can be deduced from basic soil properties or hydrograph analysis as described in Kneis (2012a). To facilitate the identification of physically reasonable, near-optimum parameter values multiple objective functions may be evaluated simultaneously. In this study, both the Nash–Sutcliffe Index and the percentage bias were used (Eqs. 4 and 5). In addition, the two objective functions were analyzed for subsets of observations (low flow, high flows, full range). The analysis of the model error during periods of low flow was essential for identifying the parameters that control groundwater recharge and drainage.

The described methodology may be regarded as a stochastic algorithm with regular human intervention. The SMCS approach is believed to be a reasonable generic alternative to other strategies. Compared to manual calibration, for example, the SMCS reduces the manual effort dramatically and it leaves less room for subjectivity. Compared to fully automatic optimization, the SMCS is robust as it bypasses typical numerical obstacles. In this case study, a total of 800–1000 model runs was needed to calibrate the model for a single gaged sub-basin.

HESSD
11, 1169–1201, 2014

3.3.6 Model validation

Typically, only some part of an observed hydrograph is used for model calibration while the other part is reserved for validation. In this case study, however, the split-sample approach was found to be very sensitive to the choice of the particular time periods used for calibration and validation, respectively. Therefore, an alternative strategy of model validation was adopted where the calibrated parameter sets are exchanged between neighboring catchments. This strategy analyzes the parameter's transferability in space rather than time.

The validation experiments were carried out using the rain gage data (Sect. 3.1.2) as precipitation forcing. The results are summarized in Tables 6 and 7. The original performance of the calibrated model is represented by the bold numbers. Normal-face numbers off the diagonals indicate the performance when the calibrated parameters from a particular catchment (specified in the the row header) are applied to a different catchment (column header).

According to the statistics presented in Tables 6 and 7, the model concept is capable of capturing the catchment's fundamental hydrological behavior. Hence, the model was also used to analyze the impact of different precipitation inputs (Sect. 3.2)

4 Results

4.1 Daily areal precipitation estimates

The correspondence between TRMM precipitation estimates and ground data was analyzed for five major sub-catchments (cf. Fig. 1). Assuming the rain gage-based estimates to be reliable, the TRMM data reflect about 60–70 % of the observed variance in daily areal rainfall (Table 8). Compared to the post-processed product, the real time data perform worse. In particular, the real-time data which did not undergo bias correction exhibit a consistent underestimation (rightmost column of Table 8).

HESSD
11, 1169–1201, 2014

The representation of high rainfall intensities by the TRMM data is examined in Fig. 3. In all investigated sub-catchments, the POD shows a steep decline towards higher rainfall intensities. While scores of 0.6–0.8 were found for low intensities, typical POD values range from 0.2–0.5 for events exceeding the threshold of 100 mm day^{-1}. In general, higher scores were obtained for the gage-adjusted TRMM product (SG) as compared to the raw real-time product (SRR).

False alarm ratios fall in the range from 0.2 to 0.6. As opposed to the POD statistics, the FAR is not strongly correlated with the threshold intensity. There is also no clear ranking with respect to the compared TRMM products.

According to the equitable threat score (ETS), the two compared TRMM products perform more or less similar. The declining graphs in the bottom row of Fig. 3 underpin the general deterioration of the precipitation estimates if the focus of interest is shifted towards more extreme events.

4.2 Simulated runoff for different rainfall estimates

The quality of stream flow simulations with different precipitation estimates is summarized in Table 9. Except for the numbers in parenthesis, all results were obtained with model parameters optimized for the respective rainfall forcing. It has to be noted that the flow rates at Tikarpara and Mundali are heavily influenced by the release from the Hirakud dam. Consequently, the simulated discharge at these two gages is naturally less sensitive to the model's rainfall input.

According to Table 9, the match between simulated and observed stream flow is generally higher for the rain gage data (G24, G3) as compared to the TRMM estimates (SG, SRC). For the two gage-based data sets, the difference in performance was found to be week. Only for the smallest sub-catchment (cf. Table 5), the disaggregated 3 hourly data (G3) clearly seem to outperform the daily data (G24). At all but one gage, the gage-adjusted TRMM data (SG) allowed for a slightly better fit of the hydrological model than the bias-corrected real-time TRMM data (SRC).

HESSD
11, 1169–1201, 2014

A closer look at Table 9 reveals that the mentioned differences in model performance are reproduced, even if the model is not re-calibrated to the individual precipitation estimates (numbers in parenthesis). Nevertheless, it becomes obvious that re-calibration is necessary to achieve the best possible fit.

A graphical representation of Table 9 (without numbers in parenthesis) is provided as Fig. 4. In addition to the overall Nash–Sutcliffe Indices (bars), the figure also illustrates the inter-annual variability of the goodness-of-fit.

The bias corresponding to the Nash–Sutcliffe Indices reported in Table 9 is usually small. In all cases where the model was calibrated to the respective rainfall input, the percentage bias is almost negligible (< 2 %, except for Mundali). However, significant negative biases of up to −25 % were obtained for the cases where the model was fed with TRMM data but it's parameters were optimized for rain gage input (G3).

Apart from a quantitative assessment of the goodness-of-fit (Table 9, Fig. 4), it is quite informative to visually inspect model outputs for selected events and sites. Here, simulation results are presented for the annual maximum floods at Kantamal (Fig. 5). While the hydrographs produced with rain gage data (G24, G3) seem to outperform the satellite-based counterparts (SG, SRC) in years like 2007 and 2008, the picture is less clear in other years (e.g. 2003, 2005, and 2006).

5 Discussion

According to the results presented in Sect. 4.1, the TRMM precipitation estimates are only moderately correlated with ground observations (Table 8). This is so, even though the analysis was carried out on the daily scale and for spatially aggregated data. The evaluation of the POD and FAR scores (Fig. 3) suggests that the TRMM data suffer from a severe underestimation of higher rainfall intensities at the basin scale. At the same time, rainfall amounts are frequently overestimated across the whole range of intensities.

HESSD
11, 1169–1201, 2014

One has to keep in mind that areal precipitation estimates derived from local observations were used as the reference data set. This *ground truth* itself may be subject to uncertainty owing to errors in recording and deficits of regionalization, for example. Because of the rather dense network of rain gages (cf. Fig. 2), however, there is a good chance that ground truth is worthy of that name in the majority of cases. This assumption is finally supported by the results of the hydrological validation (Sect. 4.2).

In the hydrological simulation experiments, the closest agreement between observed and simulated discharges was obtained using the rain gage data as model input (Table 9, Fig. 4). With the exception of the smallest sub-catchment (gage Salebhata), the temporal resolution of the rainfall time series (3 h vs. 24 h) was found to be of little influence. On the one hand this might be explained by the smoothing effects of spatial averaging or retention becoming more important at larger scales. On the other hand, the chosen approach to disaggregation might not always be accurate enough.

As already expected from the analysis of areal precipitation estimates, the satellite-based data generally performed worse than the rain gage data. Furthermore, a consistent difference in the quality of simulated discharge was observed for the gage-adjusted TRMM data and the real-time data. The latter performed worse at all but one gage. Apparently, the monthly gage-adjustment and/or the more advanced calibration of the microwave sensors applied to the 3B42 product (Huffman and Bolvin, 2013) contribute to the quality of precipitation estimates in a significant way.

It is well known that the choice of parameter values can partly compensate for errors in a hydrological model's precipitation input (Heistermann and Kneis, 2011). Hence, there is no guarantee that a difference in the quality of two precipitation estimates can be inferred from a comparison of the errors in simulated runoff. Fortunately, the studied case appears to be well-behaved in the sense that the findings of hydrological validation (Sect. 4.2) are in good agreement with the analysis of the rainfall data alone (Sect. 4.1). Furthermore, the ranking of the precipitation estimates according to the error in simulated runoff was reproducible for different model parameterizations (Table 9).

HESSD
11, 1169–1201, 2014

Although the results of the hydrological simulations seem plausible and consistent, a number of deficits in both the hydrological model and data is known. For example, the various effects of irrigation (withdrawal of river water, evapotranspiration from impounded rice fields) are not currently simulated due to missing quantitative information. In addition, calibration and validation of the hydrological model are negatively affected by the low temporal resolution or sampling frequencies of hydro-meteorological data. Last but not least, one has to expect significant errors in stream flow data due to (very) wide gaging cross-sections in non-consolidated river beds.

6 Conclusions

The quality of satellite-based, 3 hourly precipitation estimates produced by the tropical rainfall measuring mission was examined for a part of the Mahanadi River Basin. The direct comparison of the remote sensing data with ground observations and the conducted hydrological simulation experiments yielded a consistent sight on data quality. According to the analyzed statistics, the satellite-based precipitation estimates suffer from deficiencies in the registration of intense rainfall events. At the same time, the remote sensing data frequently overestimate rainfall amounts observed at the ground. In accordance with expectations, the real-time estimates (3B42-RT product) were found to be more uncertain than the gage-adjusted 3B42 estimates which are disseminated with a delay of a few months. For the study area, the real-time data took profit from a simple bias correction. However, the remaining random errors still exceeded those of the retrospective 3B42 estimates.

The conclusions drawn from the statistical analyses do not necessarily apply to individual events. Although the remotely sensed precipitation estimates often perform worse compared to those inferred from rain gages, the opposite was found to be true in some cases. Further analyses are required to explore those instances.

The study was carried out in a catchment with a rather dense network of rain gages. It is expected that the remotely sensed precipitation estimates will be of higher "value"

HESSD
11, 1169–1201, 2014

in regions with a more sparse network of observation sites. This hypothesis might be tested, for example, by repeating the hydrological validation after "thinning out" the rain gage data base artificially. In any case, the TRMM data appear to be a reasonable source of information for "ungaged basins" in terms of rainfall.

Due to dissemination in real time, the TRMM 3B42-RT data set has the potential of being used in operational runoff prediction. This is especially interesting for regions where rain gage data are not (timely) available. An assessment of the 3B42-RT data in the context of hydrological forecasting was not part of this study. A realistic assessment would require the implementation of a framework for stream flow assimilation by the hydrological model and the evaluation of a long array of hindcasts. However, the POD and FAR scores (Fig. 3) suggest that significant forecast errors must be expected even if the hydrological model was perfectly initialized through continuous updating.

Acknowledgements. The satellite based rainfall estimates analyzed in this paper were produced and provided by the Tropical Rainfall Measuring Mission, a joint space mission between NASA and JAXA. Rain gauge and stream flow data were contributed by the India Meteorological Department and the Central Water Commission, India, respectively. The kind help of Archana Mohite and Trushnamayee Nanda in data preparation is appreciated. The first author was granted a fellowship by the German Research Foundation (ref. no. KN 884/2-1) for his stay at IIT Kharagpur.

References

Collischonn, B., Collischonn, W., and Tucci, C. E. M.: Daily hydrological modeling in the Amazon basin using TRMM rainfall estimates, J. Hydrol., 360, 207–216, 2008. 1171

de Bruin, H. A. R.: From Penman to Makkink, in: Evaporation and Weather: Proceedings and Information No. 39, edited by: Hooghart, J. C., TNO Committee on Hydrological Research, The Hague, 1987. 1191

DOWR: List of Past Flood and Area Damaged by Flood in Orissa, Tech. rep., Government of Orissa, Department of Water Resources, available at: http://www.dowrorissa.gov.in/HistoryofFLOOD/HistoryofFLOOD.pdf (last access: March 2012), 2009. 1173

HESSD
11, 1169–1201, 2014

DOWR: Annual Report 2009–2010, Tech. rep., Government of Orissa, Department of Water Resources, available at: http://www.dowrorissa.gov.in/AnnualReport/WR_AR08-09.pdf (last access: March 2012), 2010. 1173

Gao, Y. C. and Liu, M. F.: Evaluation of high-resolution satellite precipitation products using rain gauge observations over the Tibetan Plateau, Hydrol. Earth Syst. Sci., 17, 837–849, doi:10.5194/hess-17-837-2013, 2013. 1171

Heistermann, M. and Kneis, D.: Benchmarking quantitative precipitation estimation by conceptual rainfall-runoff modeling, Water Resour. Res., 47, W06514, doi:10.1029/2010WR009153, 2011. 1176, 1183

Huffman, G. J. and Bolvin, D. T.: TRMM and Other Data Precipitation Data Set Documentation, Tech. rep., Mesoscale Atmospheric Processes Laboratory, NASA Goddard Space Flight Center and Science Systems and Applications, Inc., available at: ftp://precip.gsfc.nasa.gov/pub/trmmdocs/3B42_3B43_doc.pdf (last access: 22 January 2014), 2013. 1171, 1173, 1183

Huffman, G. J., Bolvin, D. T., Nelkin, E. J., Wolff, D. B., Adler, R. F., Gu, G., Hong, Y., Bowman, K. P., and Stocker, E. F.: The TRMM Multisatellite Precipitation Analysis (TMPA): quasi-global, multiyear, combined-sensor precipitation estimates at fine scales, J. Hydrometeorol., 8, 38–55, 2007. 1171, 1173

Javanmard, S., Yatagai, A., Nodzu, M. I., BodaghJamali, J., and Kawamoto, H.: Comparing high-resolution gridded precipitation data with satellite rainfall estimates of TRMM_3B42 over Iran, Adv. Geosci., 25, 119–125, doi:10.5194/adgeo-25-119-2010, 2010. 1171

Jolliffe, I. T. and Stephenson, D. B. (Eds.): Forecast Verification, A Practitioner's Guide in Atmospheric Science, John Wiley & Sons Ltd, Chichester, West Sussex, England, 2003. 1175

JRC: Global Land Cover 2000 database, available at: http://bioval.jrc.ec.europa.eu/products/glc2000/glc2000.php (last access: 22 January 2014), 2003. 1172, 1177

Kneis, D.: Eco-Hydrological Simulation Environment (ECHSE) – Documentation of model engines, University of Potsdam, Institute of Earth- and Environmental Sciences, available at: http://echse.bitbucket.org/downloads/documentation/echse_engines_doc.pdf (last access: 22 January 2014), 2012a. 1179

Kneis, D.: Eco-Hydrological Simulation Environment (ECHSE) – Documentation of Pre- and Post-Processors, University of Potsdam, Institute of Earth- and Environmental Sciences, available at: http://echse.bitbucket.org/downloads/documentation/echse_tools_doc.pdf (last access: 22 January 2014), 2012b. 1177, 1178

HESSD
11, 1169–1201, 2014

Kneis, D., Bürger, G., and Bronstert, A.: Evaluation of medium-range runoff forecasts for a 50 km^2 watershed, J. Hydrol., 414, 341–353, doi:10.1016/j.jhydrol.2011.11.005, 2012. 1178
Li, X.-H., Zhang, Q., and Xu, C.-Y.: Suitability of the TRMM satellite rainfalls in driving a distributed hydrological model for water balance computations in Xinjiang catchment, Poyang Lake Basin, J. Hydrol., 426, 28–38, 2012. 1172
Liu, J., Zhu, A. X., and Duan, Z.: Evaluation of TRMM 3B42 precipitation product using rain gauge data in Meichuan watershed, Poyang Lake Basin, China, J. Resour. Ecol., 3, 359–366, 2012. 1171
Ludwig, K. and Bremicker, M. (Eds).: The Water Balance Model LARSIM – Design, Content and Application, vol. 22 of Freiburger Schriften zur Hydrologie, University of Freiburg, Institute of Hydrology, Freiburg, 2006. 1191
Oke, A. M. C., Frost, A. J., and Beesley, C. A.: The use of TRMM satellite data as a predictor in the spatial interpolation of daily precipitation over Australia, in: 18th World IMACS/MODSIM Congress, 13–17 July 2009, available at: http://mssanz.org.au/modsim09, Cairns, Australia, 3726–2732, 2009. 1171
Ouma, Y. O., Owiti, T., Kipkorir, E., Kibiiy, J., and Ryutaro, T.: Multitemporal comparative analysis of TRMM-3B42 satellite-estimated rainfall with surface gauge data at basin scales: daily, decadal and monthly evaluations, Int. J. Remote Sens., 33, 24, 7662–7684, 2012. 1171
Peña-Arancibia, J. L., van Dijk, A. I. J. M., Renzullo, L. J., and Mulligan, M.: Evaluation of precipitation estimation accuracy in reanalyses, satellite products, and an ensemble method for regions in Australia and South and East Asia, J. Hydrometeorol., 14, 1323–1333, doi:10.1175/JHM-D-12-0132.1, 2013. 1171
Rahman, H. and Sengupta, D.: Preliminary Comparison of Daily Rainfall from Satellites and Indian Gauge Data, CAOS Technical Report No. 2007AS1, Tech. rep., Centre for Atmospheric and Oceanic Sciences, Indian Institute of Science, Bangalore-12, 2007. 1171
Tarboton, D. G. and Luce, C. H.: Utah Energy Balance Snow Accumulation and Melt Model (UEB), Tech. rep., Utah State University and USDA Forest Service, 1996. 1191
Todini, E.: The ARNO rainfall-runoff model, J. Hydrol., 175, 339–382, 1996. 1191
Zhao, R.-J., Zuang, Y.-L., Fang, L.-R., Liu, X.-R., and Zhang, Q.-S.: The Xinanjiang model, in: Hydrological Forecasting, Proceedings of the Oxford Symposium, vol. 129 of IAHS-AISH Publ., IAHS Press, Wallingford, UK, 351–356, 1980. 1191

HESSD
11, 1169–1201, 2014

Table 1. Basic specifications of the evaluated TRMM data sets.

Data set	3B42	3B42-RT
Temporal resolution	3 h	same as left
Spatial resolution	0.25° × 0.25°	same as left
Spatial coverage	50° N–50° S	60° N–60° S
Delay of dissemination	3 months	3 h
Adjustment to gage data	Monthly sums	none
Used version	7	7, revision 2
File format (unzipped)	HDF	Custom binary format

HESSD
11, 1169–1201, 2014

Table 2. Short identifiers for the different precipitation estimates.

Abbrev.	Description
G24	Original 24 h rain gage data.
G3	3 hourly rain gage data produced by disaggregation.
SG	Gage-adjusted satellite data (TRMM 3B42).
SRR	Raw real-time satellite data (TRMM 3B42-RT).
SRC	SRR after bias correction.

HESSD
11, 1169–1201, 2014

Table 3. Contingency table to measure the correspondence between rain gage data (column headers) and remotely sensed estimates (row headers) with respect to a threshold intensity X ($\mathrm{mm\,day^{-1}}$). A value of 1 is added to the appropriate field for every analyzed event.

	Ground obs. $> X$	Ground obs. $\leq X$
Remote sens. $> X$	Hit	False alarm
Remote sens. $\leq X$	Miss	Correct negative

HESSD
11, 1169–1201, 2014

Table 4. Concepts used by HYPSO-RR to simulate major hydrological processes at the level of sub-basins, river reaches, or lakes.

Processes	Concepts
Runoff generation	– Simulation of the water balance of a single-layer soil column – Estimation of saturated areas with the Xinanjiang approach (Zhao et al., 1980) – Calculation of direct runoff using the analytical solution of Todini (1996) – Calculation of interflow and groundwater recharge as in LARSIM (Ludwig and Bremicker, 2006)
Runoff concentration	– Transformation of individual runoff components through linear reservoirs – Storage constants derived from DEM to account for spatial variability in concentration times
Evapotranspiration	– Estimation of potential evapotranspiration (PET) using the Makkink model (de Bruin, 1987) – Actual ET is derived from PET by multiplying with a soil moisture term and a crop factor – Leaf-area index is used as a proxy to capture the crop factor's seasonality
Snow storage/melt	– Energy balance model similar to the one presented in Tarboton and Luce (1996)
Channel routing	– Approximation of a uniform reach as a non-linear reservoir – Local linearization of the governing differential equation for analytical solvability – Parameters derived from cross-section data using Manning's equation
Lake storage	– Numerical solution of the water balance equation

HESSD
11, 1169–1201, 2014

Table 5. Analyzed stream gages in the central parts of the Mahanadi Basin (see Fig. 1).

Gage	River	Catchment (km^2)
Salebhata	Ong R.	4500
Kesinga	Tel R.	12 200
Kantamal	Tel R.	20 900
Tikarpara	Mahanadi	127 000
Mundali	Mahanadi	134 000

HESSD
11, 1169–1201, 2014

Table 6. Performance of the hydrological model in terms of the Nash–Sutcliffe Index (Eq. 4). Calibration results are indicated by bold-face numbers in the diagonal. Forcing: rain gage data of the period 2002–2010.

Calibrated for	Parameters applied to Salebhata	Kesinga	Kantamal
Salebhata	**0.82**	0.71	0.72
Kesinga	0.79	**0.77**	0.83
Kantamal	0.73	0.72	**0.86**

HESSD
11, 1169–1201, 2014

Table 7. Like Table 6 but numbers represent the percentage bias (Eq. 5).

Calibrated for	Parameters applied to Salebhata	Kesinga	Kantamal
Salebhata	**−1**	−14	0
Kesinga	15	**0**	16
Kantamal	−1	−13	**0**

HESSD
11, 1169–1201, 2014

Table 8. Quality of daily areal precipitation estimates gained from gage-adjusted TRMM data (SG) and raw real-time TRMM data (SRR). Reference: regionalized rain gage data.

Catchment	R^2		*p*Bias (%)	
	SG	SRR	SG	SRR
Salebhata	0.64	0.60	10	−6
Kesinga	0.71	0.68	−8	−26
Kantamal	0.73	0.72	−5	−23
Tikarpara	0.74	0.71	5	−14
Mundali	0.65	0.59	2	−16

HESSD
11, 1169–1201, 2014

Table 9. Nash–Sutcliffe Index of simulated stream flow for different precipitation estimates (labels according to Table 2). Numbers in parenthesis were obtained with the SG and SRC input, respectively, but using model parameters optimized for G3.

	Precipitation estimate			
Catchment	G24	G3	SG	SRC
Salebhata	0.82	0.86	0.71 (0.69)	0.67 (0.66)
Kesinga	0.77	0.76	0.70 (0.70)	0.65 (0.58)
Kantamal	0.87	0.88	0.78 (0.75)	0.77 (0.69)
Tikarpara	0.88	0.89	0.88 (0.90)	0.90 (0.89)
Mundali	0.94	0.93	0.88 (0.87)	0.86 (0.83)

HESSD
11, 1169–1201, 2014

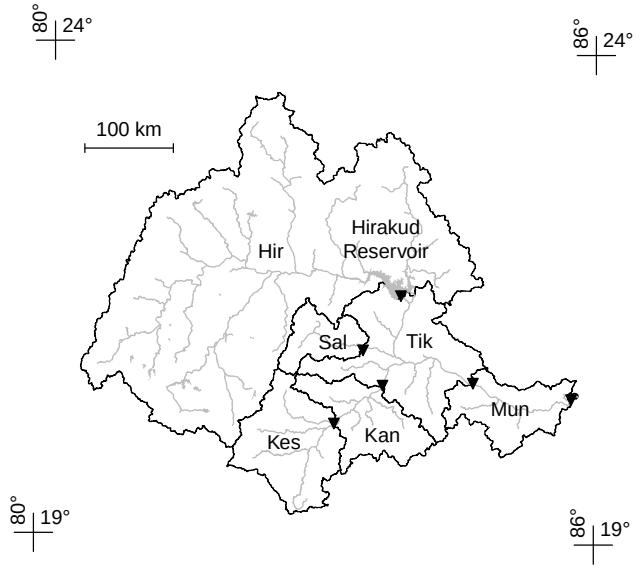

Fig. 1. Mahanadi River Basin with the analyzed gages (triangles) and their catchments. Gage names are abbreviated: Hirakud, Kesinga, Salebhata, Kantamal, Tikarpara, Mundali.

HESSD
11, 1169–1201, 2014

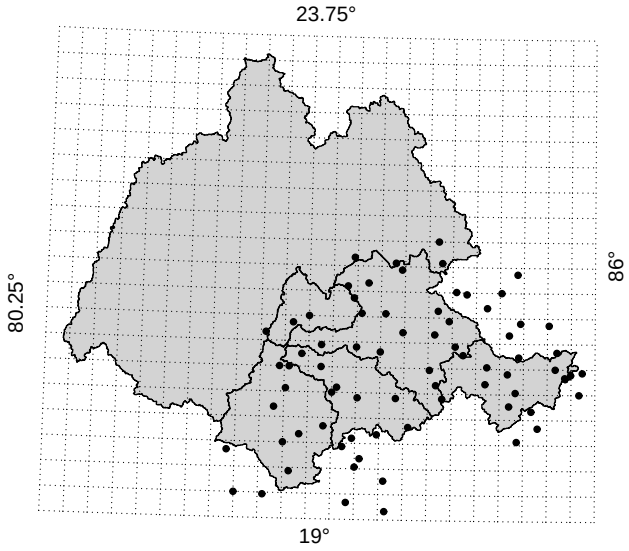

Fig. 2. Grid of the TRMM 3B42/3B42RT product covering the Mahanadi River Basin. Individual cells are 0.25° × 0.25° wide. Filled dots represent rain-gages in sub-catchments downstream of the Hirakud dam (see Fig. 1).

HESSD
11, 1169–1201, 2014

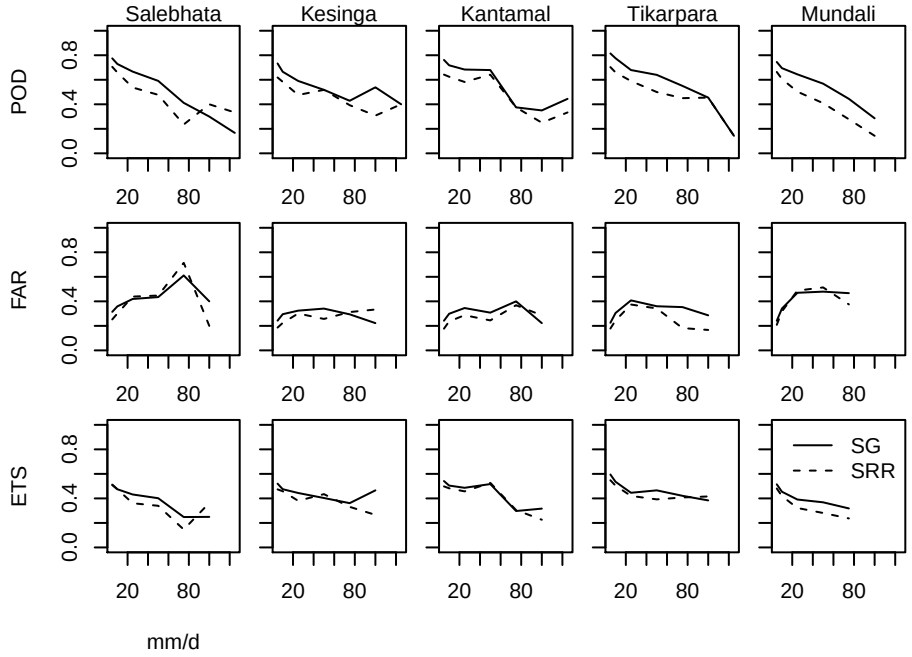

Fig. 3. Probability of detection (POD), false alarm ratio (FAR) and equitable threat score (ETS) of satellite-based estimates of daily areal precipitation for selected thresholds (x axis). Data set labels according to Table 2. Columns correspond to the sub-catchments shown in Fig. 1.

HESSD
11, 1169–1201, 2014

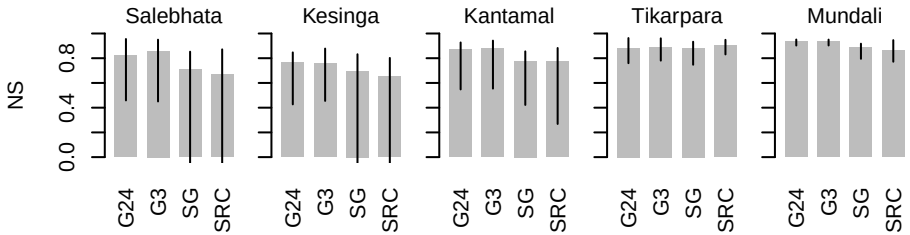

Fig. 4. Nash–Sutcliffe Indices of simulated runoff. Bars represent the values from Table 9 related to the entire evaluation period 2000–2010. Thin vertical lines indicate the range of the Nash–Sutcliffe Indices obtained for individual years (*y* axis cut off at zero).

HESSD
11, 1169–1201, 2014

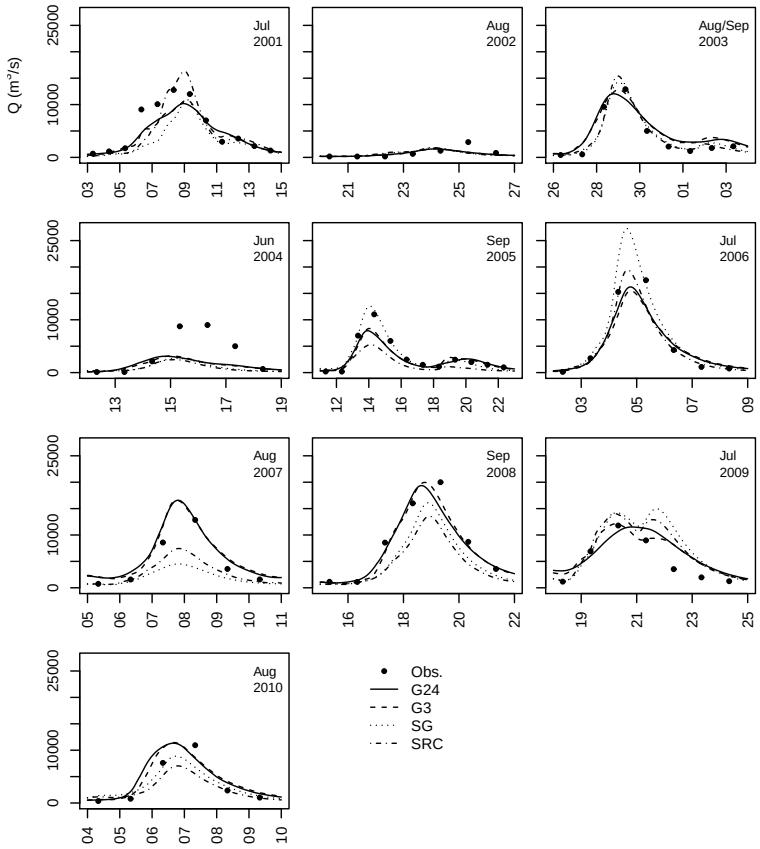

Fig. 5. Observed and simulated stream flow at Kantamal (see Fig.1, Table 5) for the annual floods in 2001–2010. *x* axis labels represent the day of the month. All *y* axis with identical scaling.

HESSD
11, 1169–1201, 2014